ADVANCED MATERIALS

Supporting Information

for *Adv. Mater.,* DOI: 10.1002/adma.202208293

Unusual Spectrally Reproducible and High Q-Factor Random Lasing in Polycrystalline Tin Perovskite Films

Vladimir S. Chirvony, Isaac Suárez, Jesus Sanchez-Diaz, Rafael S. Sánchez, Jesús Rodríguez-Romero, Iván Mora-Seró,* and Juan P. Martínez-Pastor**

SUPPORTING INFORMATION

Unusual Spectrally Reproducible and High Q-Factor Random Lasing in Polycrystalline Tin Perovskite Films

Vladimir S. Chirvony[a]*, Isaac Suárez[b], Jesus Sanchez-Diaz[c], Rafael S. Sánchez[c], Jesús Rodríguez-Romero[d], Iván Mora-Seró[c*], and Juan P. Martínez-Pastor[a]*

[a] UMDO, Instituto de Ciencia de los Materiales, Universidad de Valencia, Valencia 46980, Spain;

[b] Escuela Técnica Superior de Ingeniería, Universidad de Valencia, Valencia 46100, Spain;

[c] Institute of Advanced Materials (INAM), Universitat Jaume I, Castelló de la Plana, 12071, Spain

[d] Facultad de Química, Universidad Nacional Autónoma de México, Coyoacán, Ciudad de México 04510, Mexico.

*e-mails: vladimir.chyrvony@uv.es; sero@uji.es; martinep@uv.es

Experimental Section

Materials

Tin(II) iodide (SnI_2, 99.99%), tin(II) fluoride (SnF_2, 99%), Sodium borohydride (NaBH4, 96%), N,N-dimethylformamide (DMF, 99.8%), dimethylsulfoxide (DMSO, 99.8%), chlorobenzene (CB, 99.8%) and ethyl acetate (EtOAc, 99.8%) were purchased from Sigma-Aldrich. Formamidinium iodide (FAI, 99.99%) and methylammonium iodide (MAI, 99.99%) were purchased from Greatcell Solar Materials. All materials were use as received with no further purifications.

Dipropylammonium iodide synthesis

Dipropylammonium iodide salt (DipI) was synthesized following the procedure reported in a previous work. **[S1]** In brief, 10 g dipropylamine were added to 30 mL of cold EtOH. Then 13 mL of HI were dropwise added to the flask under vigorous stirring. The white solid formed after the addition of HI was filtered and washed with 100 mL of cold diethylether and then it was recrystallized using EtOH.

Preparation of Perovskite precursor solutions

Pristine $FASnI_3$ precursor solution: 298 mg of SnI_2 (0.8M), 137.57 mg of FAI (0.8 M) and 12.48 mg of SnF_2(0.08 M) were dissolved in 1 mL of a binary mixture of DMSO:DMF (9:1, v/v) and stirred over night at room temperature.

$FASnI_3$ precursor solution with DipI and $NaBH_4$: 298 mg of SnI_2 (0.8 M), 123.81 mg of FAI (0.72 M), 36.65 mg of DipI (0.16 M), 12.48 mg of SnF_2 (0.08 M) and 0.19 mg of $NaBH_4$

(0.005 M, may vary depending on the precursor purity, brand or Batch) were dissolved in 1 mL of a binary mixture of DMSO:DMF (9:1, v/v) and stirred over night at room temperature.

$MAPbI_3$ precursor solution: 612 mg of PbI_2 (1.3 M) and 211 mg of MAI (1.3 M) were dissolved in 1 mL of DMSO and heated at 60 ^oC for 2 hours.

Film fabrication

Films were prepared using the method recently reported in Ref. **[S2]**. Glass substrates were washed with soap-water, ethanol, acetone and isopropanol, respectively, in an ultrasonic bath for 15 minutes each of the steps. Then, the substrates were dried with N_2 flow and right before the perovskite film deposition, they were introduced in an UV-Ozone cleaner for 20 min and then the substrates were introduced in a N_2 filled glovebox. The $FASnI_3$ perovskite layer was deposited by one-step method with an antisolvent-based method, by adding $FASnI_3$ precursor solution (with or without additives) on top of glass substrate and spin-coated at 4000 rpm for 50s. Then 400 µl of chlorobenzene (CB) were dropped on top of the substrate after 20s of spinning, followed by a two-step annealing at 70 ºC for 1 minutes and at 100 ºC for 19 min. The $MAPbI_3$ perovskite layer was deposited by spin-coating 70 µl of perovskite solution at 2 ramps, 2000 rpm for 10 s and 6000 rpm for 30 s with an acceleration of 3000, ethyl-acetate was used as antisolvent at the 15^{th} second of the second ramp and then the substrate was annealed at 130 ^oC for 10 min. After the perovskite film was formed and cool down, a PMMA solution (100 mg/ml in CB) was spin-coated at 3000 rpm and 3000 of acceleration and then the substrate was annealed at 100 ^oC for 3 minutes. After the fabrication process, a 3-day light soaking treatment was made inside a N_2 filled glovebox, using an LED lamp.

The $MAPbI_3$ perovskite layer was deposited by spin-coating 70 µl of perovskite solution at 2 ramps, 2000 rpm for 10 s and 6000 rpm for 30 s with an acceleration of 3000, 450 µl of ethyl-acetate was used as antisolvent at the 15th second of the second ramp and then the substrate was annealed at 130^{o} C for 10 min.

Film characterization

SEM images were taken with a field emission scanning electron microscope (FEG-SEM) JEOL 3100F) operated at 15 kV. Absorption spectra were registered on a Varian 20Cary300 BIO UV/VIS spectrophotometer. Photoluminescence (PL) and time-resolved PL (TRPL) of thin films were realized in a closed-cycle He cryostat, which can be cooled down to 20 K. For TRPL measurements the sample were excited by a 200 fs pulsed Ti:sapphire (Coherent Mira 900D) at a repetition rate of 76 MHz doubled to 405 nm with a BBO crystal. The backscattered PL signal was dispersed by a double 0.3-m focal length grating spectrograph/spectrometer (1200 g/mm with 750 nm blaze) and detected by a Si micro photon device (MPD) and single-photon avalanche diode (SPAD) photodetector (connected through a multimode optical fiber to the monochromator); the SPAD was attached to a time correlated single photon counting electronic board (TCC900 from Edinburgh Instruments). The instrument response function is about 50 ps. For ASE/RL measurements a powerful pulsed laser was used generating 1 ns pulses at 532 or 355 nm with the pulse repetition rate of 1 kHz. The signal accumulation time during the detection of RL spectra was 20 – 500 ms, depending on the signal intensity, which corresponds to averaging over 20 – 500 laser pulses, respectively.

NOTE S1. EXCITATION GEOMETRIES

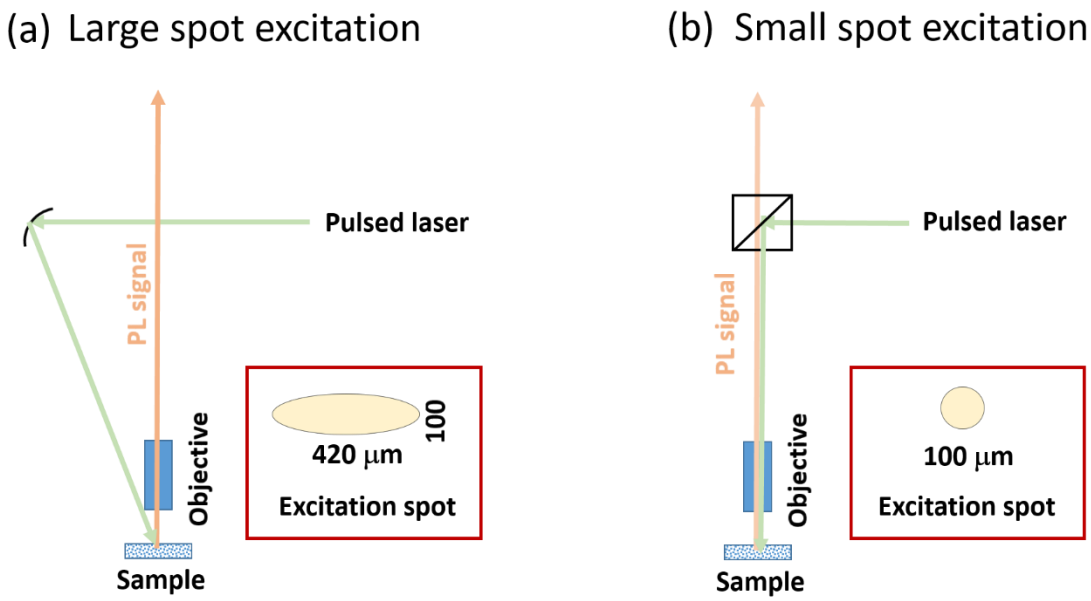

Scheme 1. Excitation geometries with (a) large and (b) small excitation spots.

For investigation of lasing properties of [$FASnI_3$] films we used excitation by powerful 1-ns laser pulses at 532 or 355 nm and detected PL signal in back-scattering geometry. Two different geometries were used, which are shown in **Scheme S1.** In the first of them, the exciting beam was directed to the sample using a focusing mirror at an angle of 30° to the sample surface (**Scheme S1a**). In this case, the excitation spot had a shape of an ellipse with diameters of 420 and 100 μm in full width at half maximum (FWHM) of the spatial profile. Photoluminescence (PL) from the sample was directed to the detection system with use of an objective. In the second case, the excitation beam was directed to the sample using a beam-splitter through the same

objective by which the PL signal was directed to the detection system (**Scheme S1b**). In this case, the excitation spot was in a form of a circle with the diameter of 100 μm. We used these two different types of the excitation spots in our experiments, since it is known from the literature that the parameters of enhanced luminescence and random lasing can strongly depend on the size and shape of the excitation spot on sample. **[S3]** In the first part of the work we used the large excitation spot (420x100 μm ellipse). It is in this geometry where we obtained the lowest thresholds for ASE and RL. In the second part of the manuscript, the small area excitation spot (100 μm circle) was used. We performed measurements at room temperature and 20 K, since the thresholds for enhanced PL and RL as well quality factor Q are sensitive to the temperature-induced spectral broadening and non-radiative recombination.

NOTE S1b. Photophysical properties of $FASnI_3$

The photophysics of tin-based halide perovskites is quite different from that of analogous Pb-based perovskites. In particular, it has been demonstrated that when the Sn^{2+} ion is oxidized to Sn^{4+}, the Sn^{4+} acts as a p-type dopant within the material in a process referred to as "self-doping" **[S4, S5]**. High unintentional doping is unwanted in photovoltaics because it causes fast band-to-band recombination of carriers (with characteristic lifetimes of tens - hundreds of picoseconds) **[S6]** and, consequently, short diffusion lengths (tens of nanometers).

Although such p-doping is clearly detrimental for photovoltaics, the doping can be advantageous for lasing applications because the additional monomolecular recombination pathway between photoexcited electrons and holes released from dopants should be radiative for a direct band gap semiconductor **[S7]**. Few direct experimental data also support increased radiative efficiency in Sn-doped perovskites: it was found, for example, that in case of Sn-based

perovskite thin films PLQY is more than one order of magnitude higher than for analogous Pb-based perovskite films **[S8]**.

Until now the number of experimental studies of near-infrared ASE and/or lasing in Sn iodide perovskite thin films is very limited **[S7, S9, S10, S11]**. In all these works, the authors used ~ 10-20% SnF_2 additive to reduce self-p-doping, which made it possible to increase the PL lifetime from the initial tens of picoseconds to ~ 0.5 ns and thus improve the conditions for observing ASE or lasing **[S12]**.

In case of our $FASnI_3$ samples, we also used 10% SnF_2 additive to reduce self-p-doping, which enabled us to increase PL lifetime up to ~ 0.5 ns (without additives) and then further increase it to ≈ 1.5 ns after addition of anti-oxidant agent ($NaBH_4$) and a passivating additive, dipropylammonium iodide (DipI) as well as an additional light treatment (soaking), as it is describe in Experimental Section in Supporting Information. We suggest that the found independence of PL lifetime of $FASnI_3$ samples on temperature can be related to the p-doped character of this material, although additional photophysical investigations are required.

FIGURES

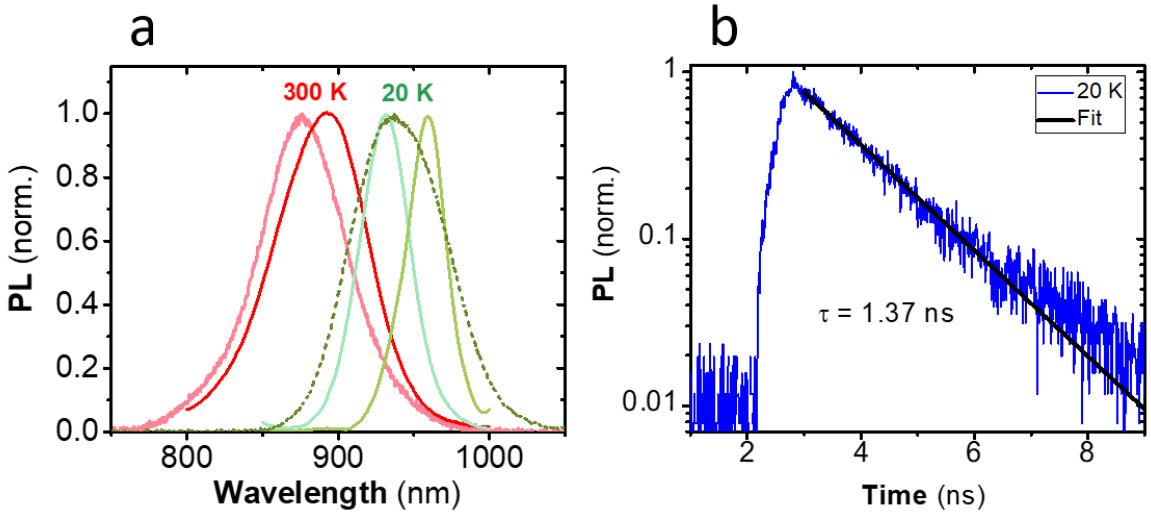

Figure S1. PL characterization of $FASnI_3$ film on glass under low intensity excitation. (a) Typical PL spectra measured at 300 K (red colors) and 20 K (green colors); (b) PL kinetics measured at 20 K (detection at 930 nm). Different colors of PL spectra correspond to excitation in different places of a sample.

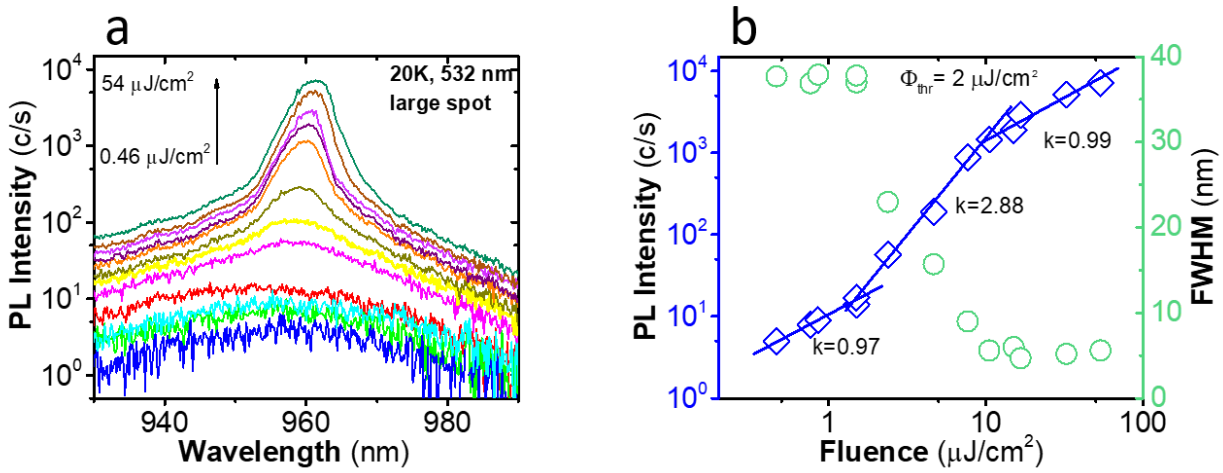

Figure S2. (a) PL spectra of $FASnI_3$ thin films on glass measured at 20 K at different excitation fluences with excitation by 532 nm pulses with a large spot; (b) the corresponding presentation of the PL intensity and FWHM dependences on excitation fluence.

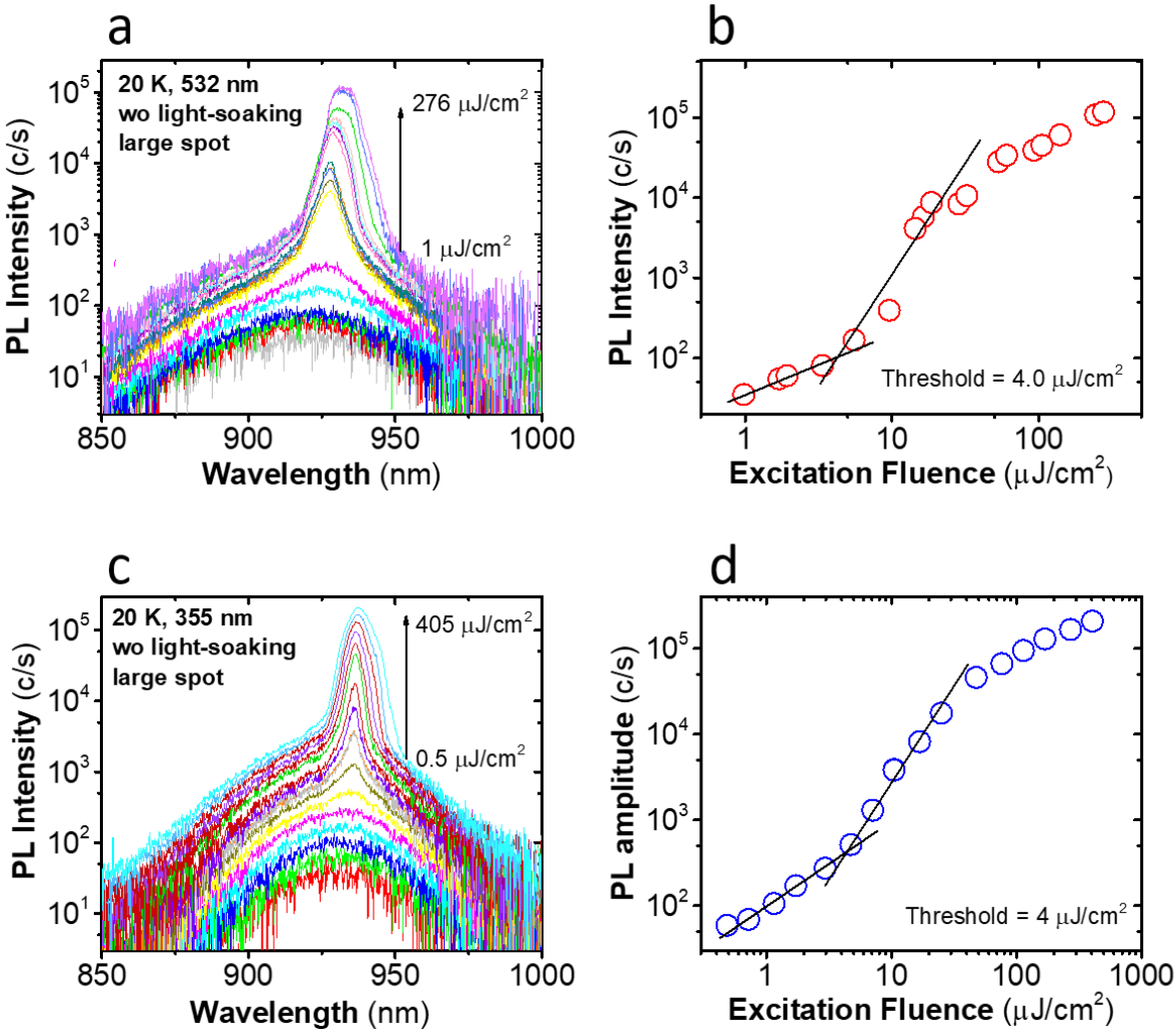

Figure S3. (a, c) PL spectra of two different $FASnI_3$ thin films on glass prepared without light-soaking and measured at 20 K at different excitation fluences with excitation by 532 nm (a) and 355 nm (c) pulses; (b, d) log-log presentations of the corresponding PL intensity dependences on excitation fluence.

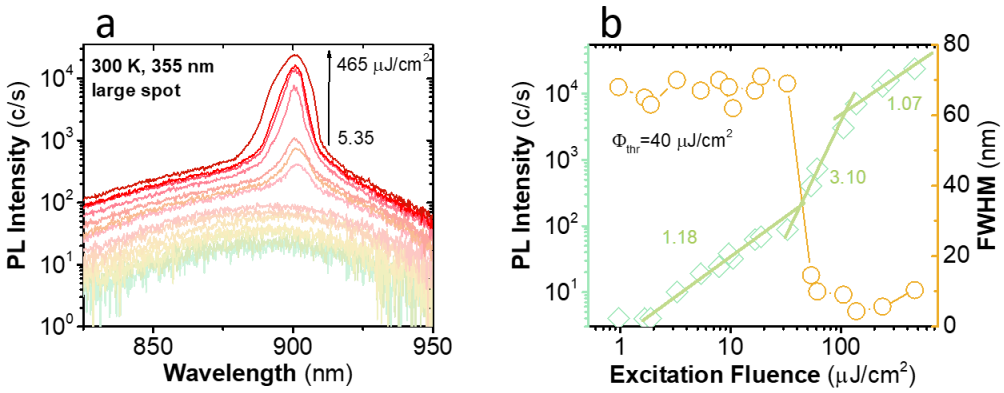

Figure S4. (a) PL spectra of $FASnI_3$ thin films on glass measured at 300 K at different excitation fluences with excitation by 355 nm pulses with a large spot; (b) the corresponding presentation of the PL amplitude and FWHM dependences on excitation fluence.

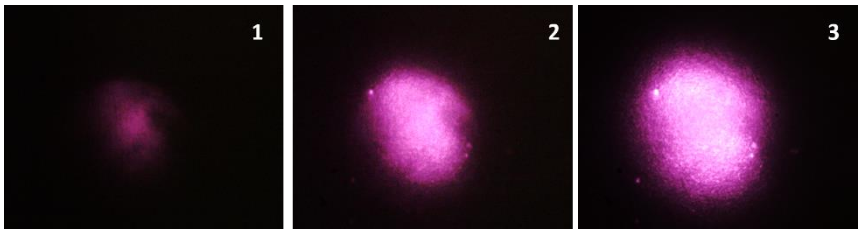

Figure S5. Images of PL spots from a $FASnI_3$ thin film detected under increasing excitation fluence, from 1 to 3.

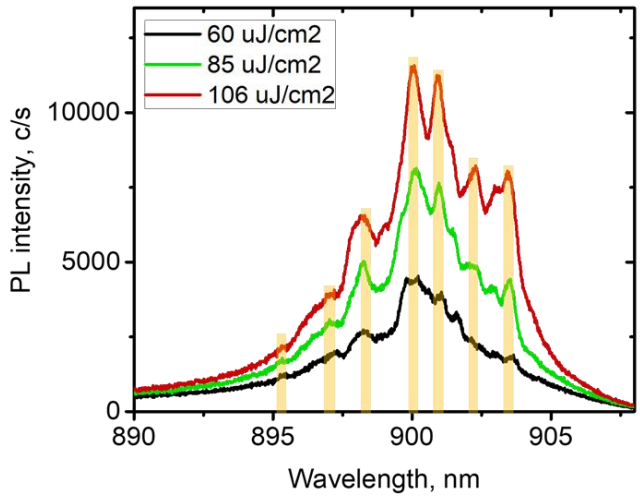

Figure S5b. RL spectra of $FASnI_3$ films measured at room temperature with large-spot excitation at 355 nm with different fluences (indicated in the legend).

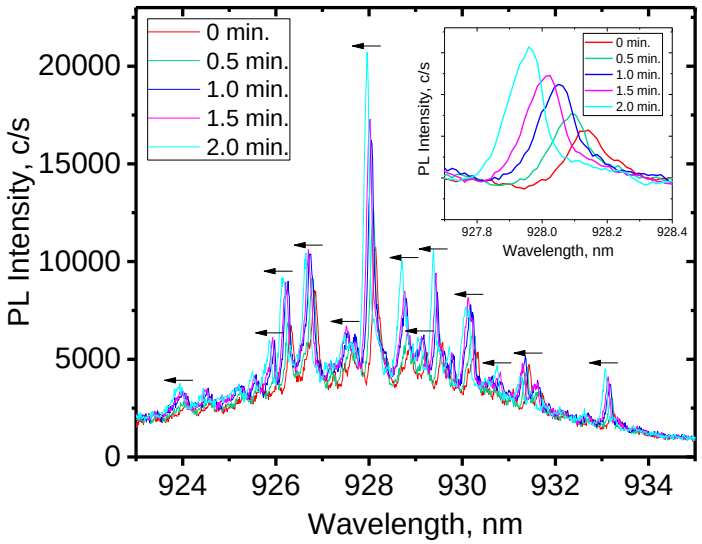

Figure S5c. RL spectra of $FASnI_3$ films at 20 K detected with 30 s interval after each other. Excitation by 1-ns 355 nm pulses. The inset shows a narrow spectral interval around the most intensive line at 928 nm.

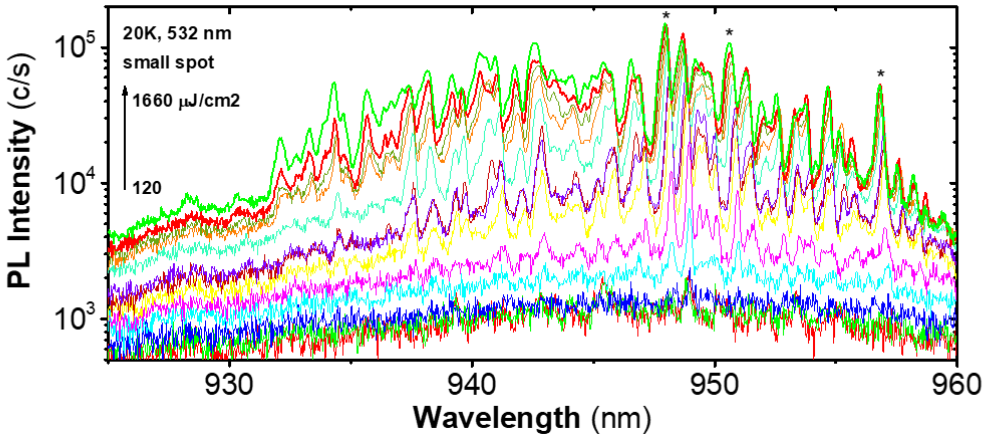

Figure S6. PL spectra of $FASnI_3$ thin films on glass measured at 20 K at different excitation fluences with excitation by 532 nm pulses with a small spot. Lines indicated with asterisks are analyzed in **Figure 4c**.

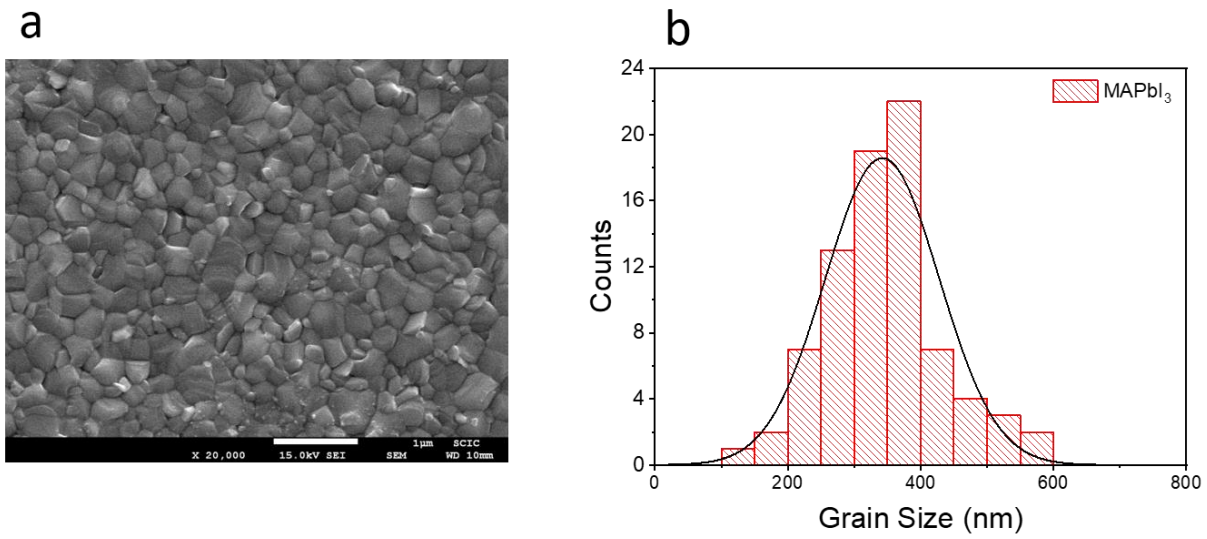

Figure S7. (a) SEM image and (b) grain size distribution for $MAPbI_3$ thin polycrystalline film.

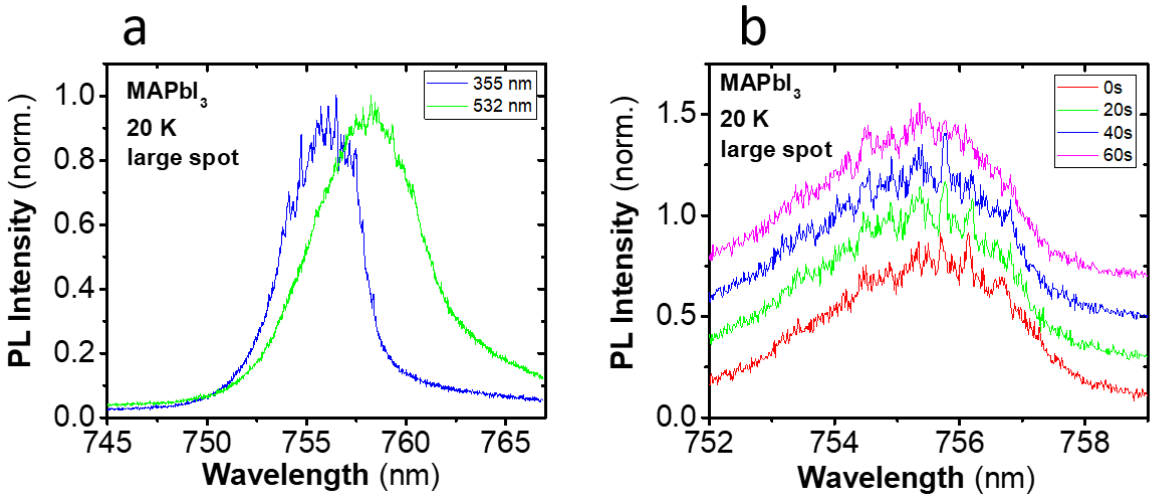

Figure S8. PL spectra of thin $MAPbI_3$ films excited at 20 K by 1-ns pulses; (a) normalized spectra excited at 355 nm and 532 nm; (b) four PL spectra excited at 355 nm and measured 20 s after each other.

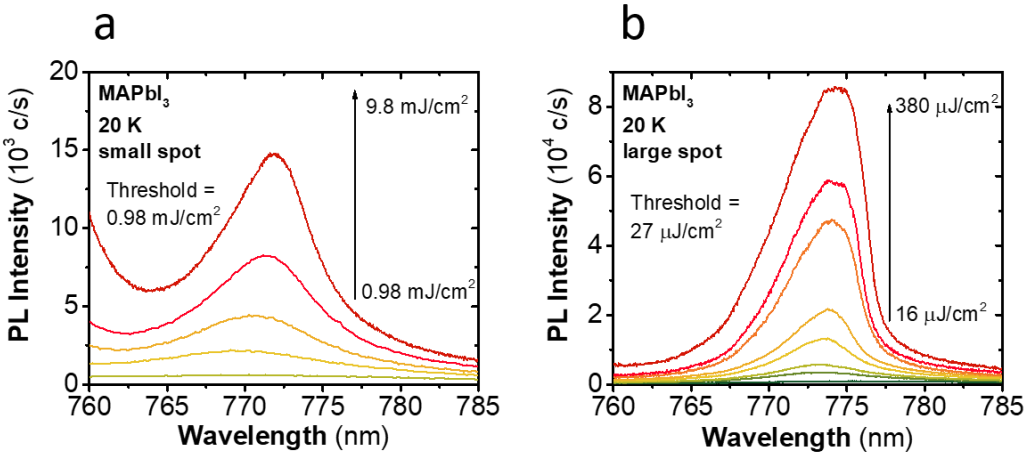

Figure S9. PL spectra of $MAPbI_3$ thin film measured at 20 K under small (a) and large (b) spot excitation by 532 nm pulses at different excitation fluences.

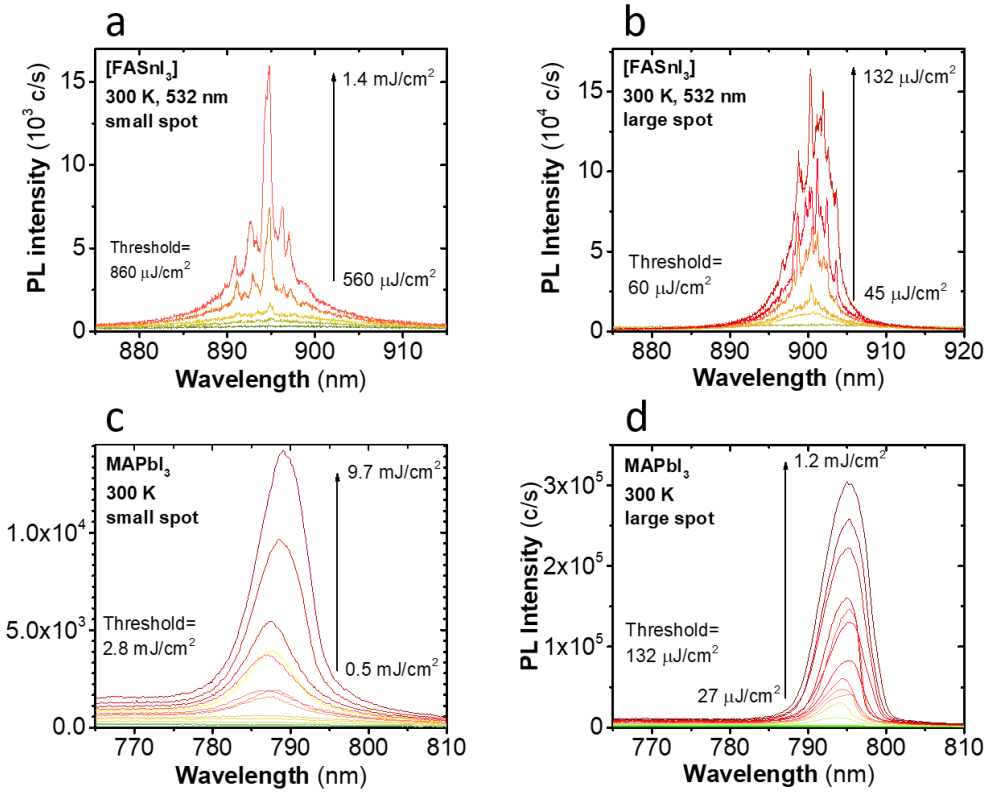

Figure S10. Room temperature ASE/RL spectra of $FASnI_3$ (a, b) and $MAPbI_3$ (c, d) films excited at 532 nm by small (a, c) and large (b, d) excitation spot.

NOTE S2. Investigation of $FASnI_3$ samples with modified morphology

We also performed experiments to shed light on the role of $FASnI_3$ films morphology in the observed RL effects. To do this, we slightly modified the protocol for obtaining polycrystalline films, which allowed us to reduce the grain size in the films and also modify the grain packing density. The standard procedure for obtaining polycrystalline perovskite films on a substrate surface is as follows. A small amount of a solution of $FASnI_3$ in a mixture of solvents (DMSO:DMF) is placed with a pipette on a substrate mounted on a spin-coater, after which its rotation is started. After a strictly defined time Δt after the start of rotation, which we call "antisolvent time", a certain amount of an "antisolvent" (in this case chlorobenzene was used) is dropped onto the surface of the substrate with a solution of $FASnI_3$, which leads to rapid crystallization of $FASnI_3$ in the form of a film on the surface and evaporation of solvents. By varying Δt, it turned out to be possible to vary the grain size, as well as their packaging density. All previous experiments in this work were performed at Δt = 20 s, when large $FASnI_3$ grains with an average size of about 800 – 1000 nm were formed, closely adjacent to each other, **Fig. 1 a, b**. An increase in Δt to 35 s made it possible to reduce the average grain size to about 500 nm, **Figure S11**), while the grain packing becomes less dense and numerous pinholes appear. Next, we performed experiments to determine the ASE threshold and RL line spacing for $FASnI_3$ films prepared from the same stock solution, but at Δt = 20 s (sample $FASnI_3$ (20s), **Figure S12**) and Δt = 35 s (sample $FASnI_3$ (35s), **Figure S13**).

Our studies have shown that for the sample $FASnI_3$ (20s), **Figure S12**, ASE threshold is about 5 $\mu J/cm^2$ and the average RL spacing is about 0.3 nm. In turn, for the sample $FASnI_3$ (35s), **Figure S13**, ASE threshold is essentially higher, about 25 $\mu J/cm^2$ and the average RL spacing

does not change as compared to 20s and again is about 0.3 nm. Thus, the grain packing density and, possibly, their average size affect the generation threshold, but not the quality of narrow RL lines.

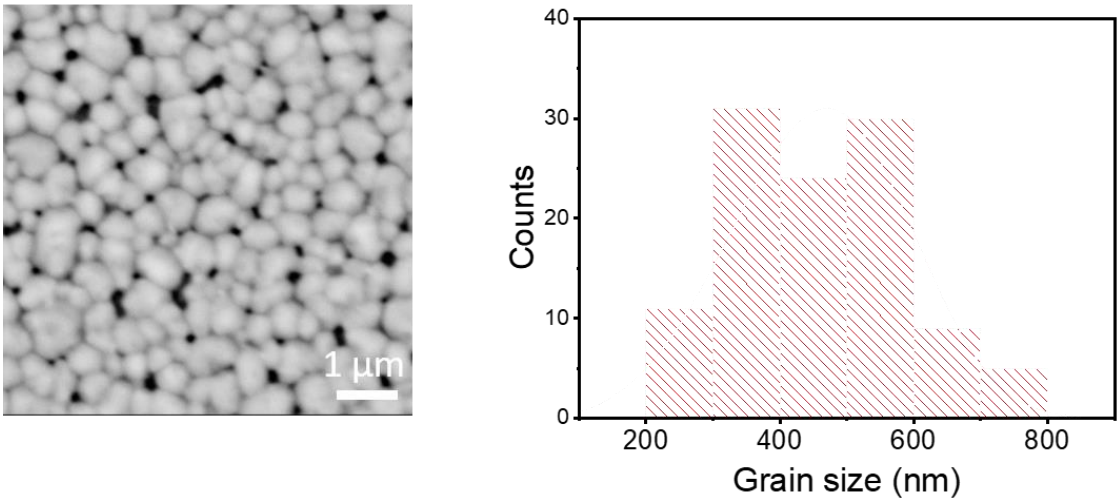

Figure S11. SEM image and grain size distribution (scale bar is 1 μm) for $FASnI_3$ films prepared with Δt = 35 s.

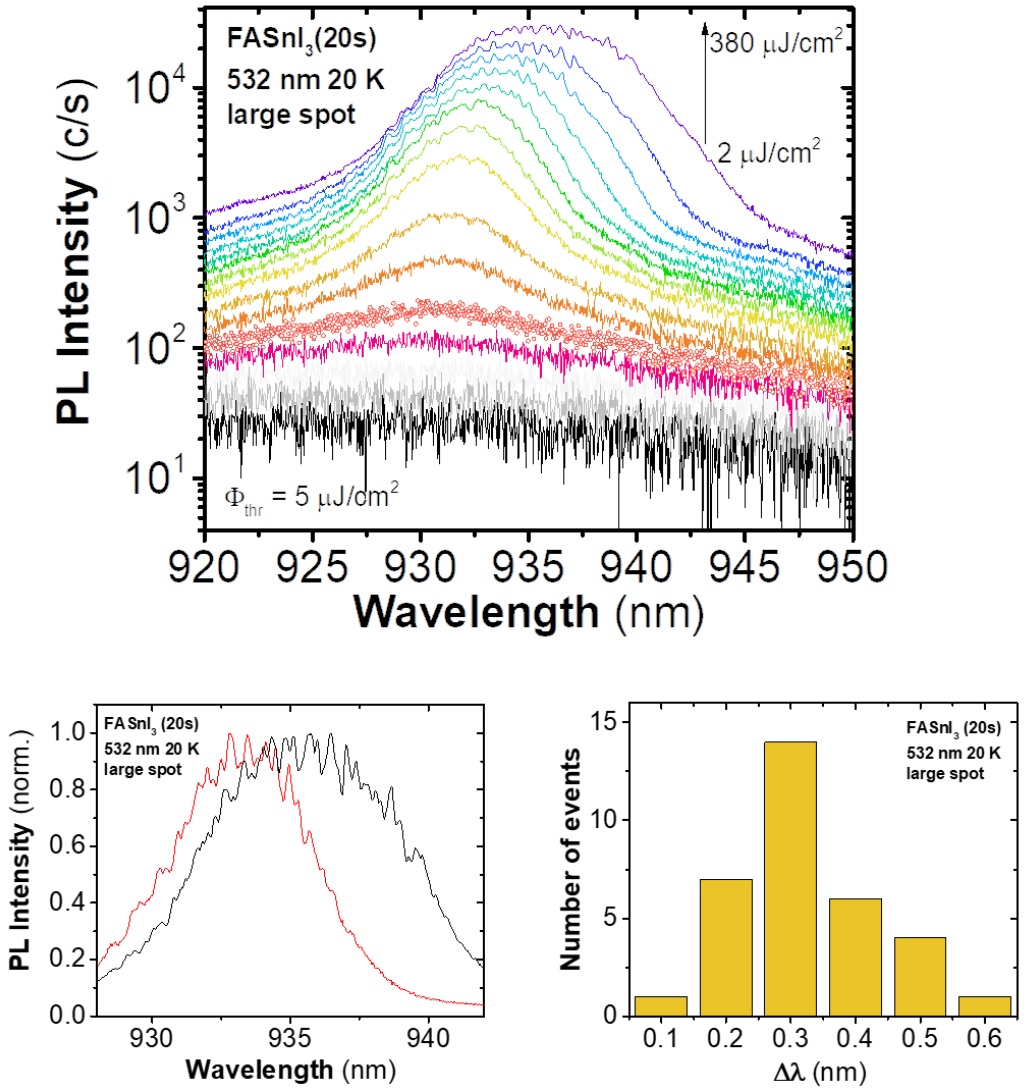

Figure S12. (top) PL spectra of $FASnI_3$ thin films on glass, Δt = 20s, measured at 20 K at different excitation fluences with excitation by 532 nm pulses with a large spot; (bottom left) PL spectra measured at 20 K with a large excitation spot, which were used to determine the mode spacing distribution (bottom right).

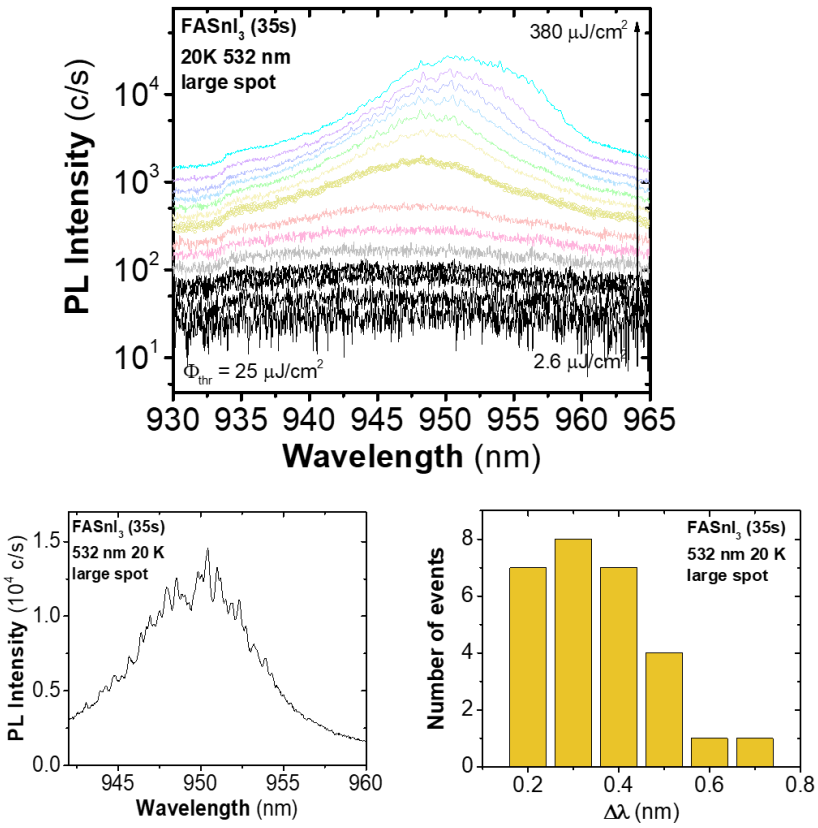

Figure S13. (top) PL spectra of $FASnI_3$ thin films on glass, Δt = 35 s, measured at 20 K at different excitation fluences with excitation by 532 nm pulses with a large spot; (bottom left) PL spectra measured at 20 K with a large excitation spot, which were used to determine the mode spacing distribution (bottom right).

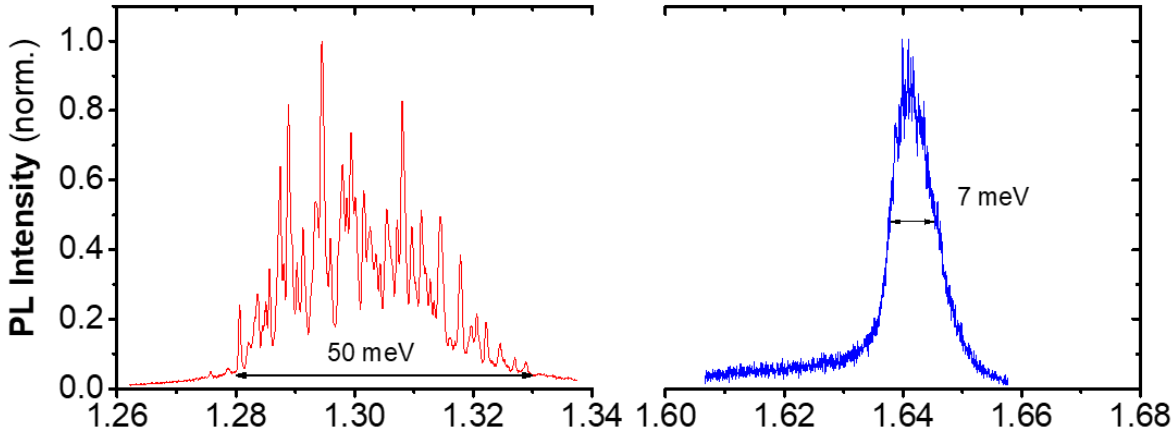

Figure S14. Comparison of typical RL spectra of $FASnI_3$ (red) and $MAPbI_3$ (blue) films detected at 20 K.

REFERENCES

S1. J. Rodríguez-Romero, J. Sanchez-Diaz, C. Echeverría-Arrondo, S. Masi, D. Esparza, E. M. Barea, I. Mora-Seró. Widening the 2D/3D Perovskite Family for Efficient and Thermal-Resistant Solar Cells by the Use of Secondary Ammonium Cations. *ACS Energy Lett.* **2020**, *5*, 1013-1021.

S2. J. Sanchez-Diaz, R. S. Sánchez, S. Masi, M. Krečmarova, A. O. Alvarez, E. M. Barea, J. Rodriguez-Romero, V.S. Chirvony, J. F. Sánchez-Royo, J. P. Martinez-Pastor, I. Mora-Seró. Tin Perovskite Solar Cells with >1,300 h of Operational Stability in N_2 Through a Synergistic Chemical Engineering Approach. *Joule* **2022**, 6, 1-23.

S3. M. Leonetti, C. Conti, C. Lopez. The mode-locking transition of random lasers. *Nat. Photonics* **2011**, *5*, 615-617.

S4. Y. Takahashi, R. Obara, Z.-Z. Lin, Y. Takahashi, T. Naito, T. Inabe, S. Ishibashi, K. Terakura. Charge-transport in tin-iodide perovskite $CH_3NH_3SnI_3$: origin of high conductivity. *Dalton Trans.* **2011**, *40*, 5563.

S5. D. B. Mitzi, C. A. Field, Z. Schlesinger, R. B. Laibowitz. Transport, Optical, and Magnetic Properties of the Conducting Halide Perovskite $CH_3NH_3SnI_3$. *J. Sol. State Chem.* **1995**, *114*, 159.

S6. L. M. Herz. Charge-Carrier Mobilities in Metal Halide Perovskites: Fundamental Mechanisms and Limits. *ACS Energy Lett.* **2017**, *2*, 1539.

S7. R. L. Milot, G. E. Eperon, T. Green, H. J. Snaith, M. B. Johnston, L. M. Herz. Radiative Monomolecular Recombination Boosts Amplified Spontaneous Emission in $HC(NH_2)_2SnI_3$ Perovskite Films. *J. Phys. Chem. Lett.* **2016**, *7*, 4178.

S8. E. S. Parrott, T. Green, R. L. Milot, M. B. Johnston, H. J. Snaith, L. M. Herz. Interplay of Structural and Optoelectronic Properties in Formamidinium Mixed Tin–Lead Triiodide Perovskites. *Adv. Funct. Mater.* **2018**, *28,* 1802803.

S9. P. Ščajev, R. Aleksiejūnas, P. Baronas, D. Litvinas, M. Kolenda, C. Qin, T. Fujihara, T. Matsushima, C. Adachi, S. Juršėnas. Carrier Recombination and Diffusion in Wet-Cast Tin Iodide Perovskite Layers Under High Intensity Photoexcitation. *J. Phys. Chem. C* **2019**, *123,* 19275.

S10. Xing, G.; Kumar, M. H.; Chong, W. K.; Liu, X.; Cai, Y.; Ding, H.; Asta, M.; Grätzel, M.; Mhaisalkar, S.; Mathews, N.; et al. Solution-Processed Tin-Based Perovskite for Near-Infrared Lasing. *Adv. Mater.* **2016**, *28,* 8191.

S11. Z. Y. Wu, Y. Y. Chen, L.-J. Lin, H.-C. Hsu. Room-Temperature Near-Infrared Random Lasing with Tin-Based Perovskites Prepared by CVD Processing. *J. Phys. Chem. C* **2021**, *125*, 5180.

S12. R. L. Milot, M. T. Klug, C. L. Davies, Z. Wang, H. Kraus, H. J. Snaith, M. B. Johnston, L. M. Herz. The Effects of Doping Density and Temperature on the Optoelectronic Properties of Formamidinium Tin Triiodide Thin Films. *Adv. Mater.* **2018**, *30*, 1804506.